Modelling of Heat Transfer in a Trapezoidal Cavity Receiver for a Linear Fresnel Solar Collector with Fixed / Narrow Reflectors

Alireza Shantia[1], Dr. Hamid Kayal[2] and Prof. Wolfgang Streicher[1]

[1] University of Innsbruck, Innsbruck (Austria). [2] csem-uae, Ras al-Khaimah (UAE)

Summary

In this research, the optical and thermal behavior of a Compact Linear Fresnel Receiver is studied with the aid of Computational Fluid Dynamics (CFD) and ray tracing methods respectively. This study aims at developing a new type of Linear Fresnel Collector (LFC) with azimuth angle tracking system. The optical analysis is performed using TracePro, a mature ray-tracing tool, in which the optical performance of the reflectors and receiver are simulated in order to obtain the optimum geometry along with the heat flux distribution on the receiver surfaces. The result of the optical analysis is used as a boundary condition for CFD modeling where the receiver located in the air stream is modeled in ANSYS Fluent. The main objectives of the thermal analysis are, firstly, to study the heat loss rate from the receiver at different absorber temperatures, and secondly, to determine the stagnation temperature under no-flow condition as an important factor contributed to thermal expansion and durability of the materials used. Further optimization is performed through examining the impact of the inner pressure and type of the gas content including air, argon and nitrogen over stratification and heat dissipation mechanism. The results indicate that a well-stablished stratification is achievable even in the atmospheric air-filled cavity. Once the conductive and convective losses are efficiently suppressed in a well-insulated receiver with a proper inner stratification state, the radiative part becomes dominant by allocating 82% of the overall heat loss. This study highlights the importance of reducing the long-wave radiative losses from the receiver to the surrounding to achieve high performance.

Keywords: computational fluid dynamics (CFD), concentrating solar power (CSP), heat transfer, linear Fresnel collector, solar thermal, thermal analysis, optical analysis
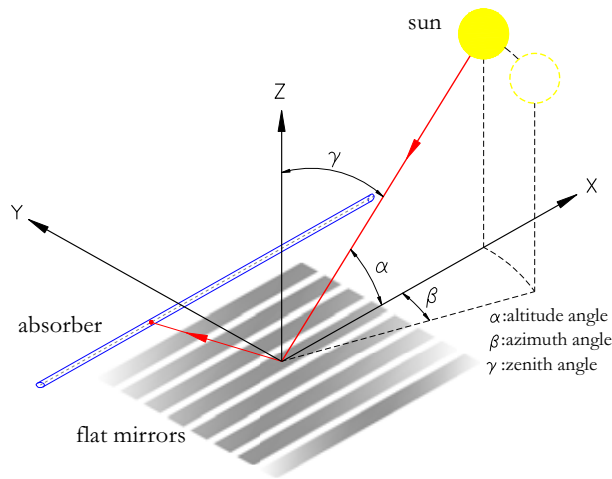
1. Introduction

Concentrating solar power (CSP) is a mature technology widely used as a reliable alternative to traditional methods that are currently used to provide high pressure and temperature for power blocks. A lot of efforts have been made across the world to make CSP technology more dependable and competitive in the energy market in terms of capacity, dispatchability, and initial / running costs. CSP technologies can be categorized into two main groups: point focusing and line focusing. Point focusing solar CSP technologies, including solar tower and solar dish, need to use two-axis tracking that makes them comparatively more complicated and expensive than other CSP technologies. In contrast, line focusing solar CSP technologies, Parabolic Trough and LFC in particular, with lower operation temperature and one-axis tracking are becoming more popular, particularly in developing countries, due to high potential for cost reduction as well as ease of manufacturing, installation and maintenance. Conventional LFC systems consist of a heliostat field equipped with one axis tracking, which reflects solar irradiation onto a stationary linear receiver positioned in the longitudinal symmetry axis of the solar array.

2. Background

This research was performed as a part of an R&D program for csem-uae (Swiss Center for Electronics and Micro technology in the United Arab Emirates) concept so-called "Solar Island" with a novel azimuth angle tracking mechanism. Solar Island is a large circular platform with rotational mechanism on a planar surface. In this tracking method, as shown in Fig.1, the mirror array and receiver are fixed on a circular structure with rotational mechanism capable of accurately tracking the sun's azimuth angle so that the azimuth angle (β in

Fig.1) is always kept nearly zero. Here, the whole platform, including the collector array, rotates horizontally to track the sun's azimuth movement contrary to conventional LFCs, in which tracking is done separately by each row of the mirror array. Thanks to this technique, the number of the moving parts are reduced to one circular disk that can lower initial and operation costs. Using fixed / narrow mirrors in this concept can also

(a) Ideal source
Altitude angle: 90,60,30,20º

(b) Sun source
Altitude angle: 90º

(c) Sun source
Altitude angle: 60º

(d) Sun source
Altitude angle: 45º

(e) Sun source
Altitude angle: 30º

(f) Sun source
Altitude angle: 20º

provide more flexibility and cost effectiveness than other LFC counterparts.

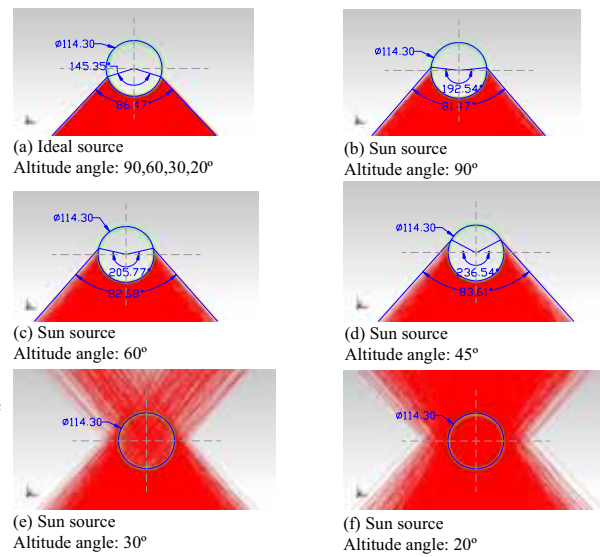**Fig.1: Azimuth angle tracking concept**   **Fig.2: Subtense angle effect on a DN100 absorber**

3. Optical Analysis

The optical analysis consists of modelling the sun as an optical source as well as optical components such as the mirror array and receiver at different altitude angles of the sun. The optical study is performed using TracePro software as a well-proved ray tracing program widely used for the optical analysis in which the so-called "Generalized Ray Tracing" technique is used for ray tracing. In TracePro, individual rays can be subject to absorption, reflection, refraction, diffraction and scatter at each intersection. Moreover, the subtense angle effect of the sun is considered in the analysis. In this case, a solar beam with an angular profile equal to that measured for the sun rays is defined in TracePro (Lambda, 2012). The optical characteristics of the csem-uae prototype are shown in Tab.1 in which the absorber tube is located 4 m vertically above the mirrors on the symmetric plane.

Tab.1: csem-uae prototype optical characteristic

Aperture width [m]	3.77
Aperture (mirror) length [m]	7.72
Receiver length [m]	13.5
Height of receiver [m]	4
Width of mirrors [mm]	Varying from inner to outer mirrors: 53, 51, 49, 47, 45
Number of mirrors [-]	59 on either side
Solar reflective area (effective mirror area) [m^2]	44.1
Mirror area / Aperture area [-]	76 %
Inclination angles of the first and the last mirrors [°]	2.81 - 21.64

The solar rays are received on the ground in a cone with the tip angle of 32', due to the subtense angle effect of the sun which remains the same for the reflected rays from a perfect mirror surface (Duffie & Beckman, 1991). Depending on the trajectory distance between each row of the mirrors and the corresponding hit points on the absorber, the subtense angle diverging effect could be significant and should be taken into account in the optical analysis.

In the Solar Island, only the azimuth angle is tracked through rotating the circular platform. Depending on

the altitude angle, measurable as the height of the sun, the impinged points of the reflected rays from the mirror field are shifted further along the absorber longitudinal axis. This in turn means a longer travel distance between the mirror and the absorber and consequently a greater divergence effect. The condition steadily deteriorates for mirrors farther from the module center. As a result, the optical concentration ratio is diminished as a larger absorber is required to collect the reflected radiation for a specific mirror array configuration.

In order to study the subtense angle effect, two light sources are defined in TracePro: ideal source and sun source. In the ideal source unlike the sun source, the angular profile of the sun is not taken into account in the optical analysis, hence as it can be seen in Fig.2a for a DN100 absorber, the results are independent from the altitude angle. The results for the sun source are also shown in Fig.2b to Fig.2.f. It can be seen that the impinged area is steadily growing by sinking the altitude angle so that the rays cannot be entirely concentrated on the absorber at the angle of 30° and lower.

The concentration ratio can be simply defined as the ratio of the aperture area to the area of the receiver (Duffie & Beckman, 1991). In linear Fresnel collectors, the aperture area is the total glass area of the primary reflectors (Weiss & Rommel, 2008). Here, the receiver area, calculated based on the impinged area on the absorber at different altitude angles, will be used for calculating the average heat flux intensity. So, we have:

$$\text{Concentration ratio} = \frac{\text{Aperture area}}{\text{Receiver area}} = \frac{\text{Total primary reflector area}}{\text{Impinged area on absorber}} \qquad \text{(eq.1)}$$

The total primary reflector area in the csem-uae prototype is 44.1 m^2 and the direct beam intensities at different altitude angles are considered for 16th June in Ras al-Khaimah in the UAE.

3.1 Optical Analysis for 2×DN50 Cavity Receiver with Actual Properties

Fig.3 shows the geometry and dimension of the 2×DN50 configuration. The outer diameter and wall thickness of the tubes are considered according to ASTM–A53 standard for SCH40 steel tubes. The insulation thickness, the hatched area in Fig.3, is initially assumed 50 mm, although it does not contribute to the optical analysis. The optical properties of the materials contributed in the optical performance are assumed as follows:

Flat mirrors: The reflection coefficient of the mirrors is provided by the manufacturer equal to 93%-94% according to the ISO9050 standard. However, since it was not possible to match the manufacture data with TracePro input parameters, the standard mirror with the closest reflection coefficient was chosen in TracePro with 0.05 and 0.948 absorption and specular reflection respectively.

Selective coating: The absorber tubes and inner parts of the cavity are covered with Black Chrome known as a well-proven selective coating material for medium and high temperature CSP applications (Forristall, 2003).

Underneath transparent cover: SCHOTT BOROFLOAT® 33 glass is used for the underneath cover due to its high transmittance, low thermal expansion and proper thermal shock resistance. Moreover, it has a lower density than the conventional soda-lime float glass and can withstand temperatures up to 450 °C (Schott, 2012). The glass thickness is assumed 5 mm in the optical analysis and the absorption coefficient of the glass
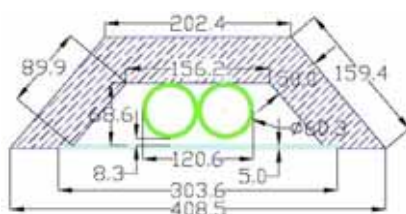
is 0.02 (Forristall, 2003). The gap between the absorber tubes and the glazing is around eight millimeters (Fig.3).

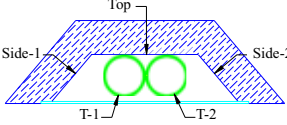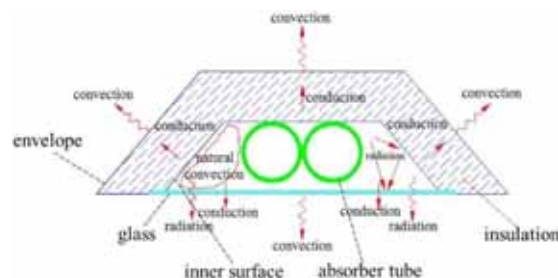Fig. 3: 2×DN50 case configuration (unit: mm)   Fig.4: Heat loss mechanism in a cavity receiver

The optical results are shown in Tab.2 and Fig.5. The heat fluxes given in Tab.2 are calculated based on the impinged area at the corresponding altitude angle. Further optical analyses were carried out for some other

alternatives with secondary reflectors inside the cavity but with the same mirror array setup. However, only a minor improvement in the optical performance was practiced owing to negligible participation of the secondary mirrors even at low altitude angles.

Tab.2: Actual power on inner surfaces of cavity

Altitude angle	Power on inner surfaces[W]					Total power[W]	Heat flux[W/m^2]		Layout
	Top	Side-1	Side-2	T-1	T-2		T-1	T-2	
90°	0.06	20.83	19.80	10656	10596	21292.6	14562	14480	
60°	0.52	18.52	17.41	8253	8190.1	16479.5	11278	11192	
45°	5.05	16.03	14.52	5688.4	5633.7	11357.7	7773	7699	
30°	56.34	19.32	19.08	2752	2729.8	5576.5	3761	3730	

Optical efficiency is an important parameter to evaluate solar collector performance. The optical efficiency and concentration ratio along with the available power on the aperture and absorber surfaces are compared in Tab.3 for different altitude angles and their corresponding beam radiations. It can be seen that the optical efficiency drops significantly at low altitude angles because of larger incident angles on the mirrors and the absorber surfaces.

Tab.3: Comparison of optical efficiency, concentration ratio and actual power on the absorber tubes

Altitude angle	Beam radiation on aperture area [W/m^2]	Total power on aperture (mirror) area [W]	Actual power on absorber tubes [W]	Optical efficiency [-]	Concentration ratio [-]
90°	546	24056	21252	88.3%	29.7
60°	488	21501	16443.1	76.5%	27.8
45°	411	18108	11322.1	62.5%	24.2
30°	285	12557	5481.8	43.6%	15.9

It should be pointed out that the absorption coefficient of the air between the mirror array and the receiver is assumed to be zero. In other words, no optical loss between the mirror and absorber is taken into account. However, in practice, part of the direct irradiance is absorbed and scattered by dust and humidity in the air. Therefore, the values given in Tab.3 must be considered as the maximum attainable power on the absorber tubes.

Altitude angle 90°   Altitude angle 90°

Altitude angle 60°   Altitude angle 60°

Altitude angle 45°   Altitude angle 45°
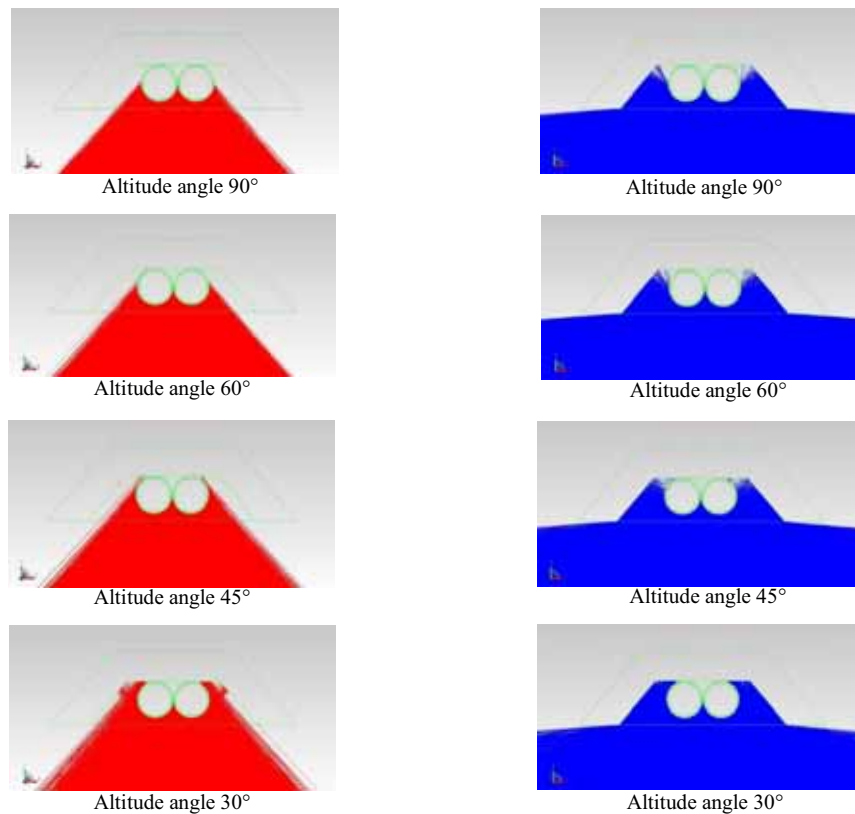
Altitude angle 30°   Altitude angle 30°

Fig.5: Optical results visualization for 2×DN50 configuration, short-wave irradiance form mirror array to receiver (left) and long-wave irradiance from optical components (right) at altitude angles: 90°, 60°, 45°, and 30°

4. Heat Loss Model

Heat loss mechanism from cavity receivers is complex and difficult to be analyzed by conventional heat transfer methods. The CFD method is implemented firstly to study the heat loss rate at different absorber temperature, and secondly to determine the stagnation temperature under no-flow condition. Further optimization will be performed through parametric study over different inner pressure and gas content including air, argon and nitrogen. Fig.4 illustrates the heat loss mechanism in a cavity receiver where natural convection and radiation losses inside the cavity are coupled with conduction through the glass and insulation along with the forced convection from the envelope to the surrounding.

4.1 Geometry and Meshing

Fig.6 shows an overall view of the mesh with a conical far-field inlet boundary and the receiver inside. The far-field boundary is extended behind the object far enough to ensure that the turbulence effect caused by the receiver is not dragged into the far-field boundary. The skewness of the mesh is kept below 0.6 in all regions.
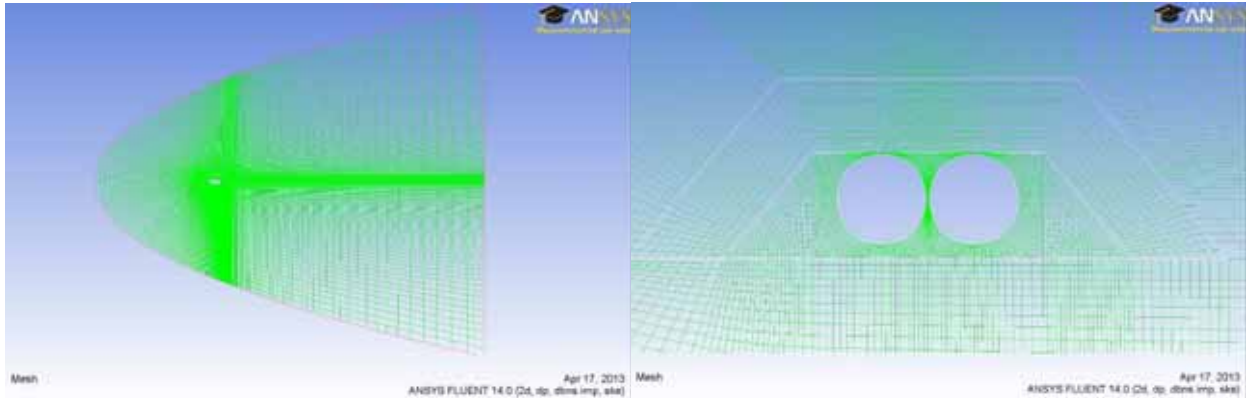

Fig.6: Mesh pattern around (left) and inside (right) of the cavity

4.2 Material Properties

Thermal properties: The specification of the materials is illustrated in Fig.7. The inner and outer surfaces of the cavity are made of aluminum sheet with a thickness of 2 mm. For the underneath transparent cover, SCHOTT BOROFLOAT® 33 glass is used. For the insulation in the upper part of the cavity, a novel insulation material for CSP applications, developed by Microtherm®, is used with a low and almost constant conductivity of 0.0227 W/m.K over a wide range of temperatures (Microtherm®, 2011).

Radiative properties: The Discrete Ordinates (DO) radiative model is used in which the optical properties such as absorption coefficient and scattering coefficient are required to calculate the radiative heat loss. The absorption coefficient is defined as the net absorbed intensity of radiation when light traverses within the material which is dependent on the optical characteristic of the material and the path length. The intensity of the transmitted radiation is decreasing continuously by the increase of the traversal path. The absorption coefficient can be calculated by the following correlation (Callister, Jr & Rethwisch, 2010):

$$\beta = -\frac{1}{x}\ln\left(\frac{I'_T}{I'_O}\right) \qquad (eq.2)$$

Where β is the absorption coefficient in 1/mm and I'_T is the intensity of the non-reflected incident radiation on the surface. I'_O is the intensity of non-absorbed radiation after traversing distance x (mm) inside the material. The distance parameter x is measured from the incident surface into the material (Callister, Jr & Rethwisch, 2010). In addition, the absorption coefficient varies with the wavelength of the incident radiation; however in the current study, it is assumed to be constant. A large β value should be considered for metals as solid and opaque materials so that the radiation energy can penetrate only a few hundred angstroms at the most. The absorption coefficient is set at 10,000 for both the absorber tubes and cavity inner surfaces to ensure that the radiation is attenuated within a very short distance (1/10,000 m = 100 μm) in the material (Shin Yee, 2006).

Air is a mixture of gases, mainly nitrogen and oxygen in addition to a little amount of other gases, which show no absorption band in the wavelength region of importance to radiant heat transfer. Nevertheless,

humidity and small particles inside the air increase the absorption coefficient in real condition. In this study, it is assumed that the cavity is charged by clean and dry air or other inert gases as it is necessary to protect the selective coating material and other inner compartments. Accordingly, the absorption coefficient of the gas content is considered to be zero in the radiant analysis. The absorption coefficient of the glass is assumed equal to 1.01E-4 (1/mm) (Callister, Jr & Rethwisch, 2010).

Solver setting: The density-based steady-state solver is used to solve the governing equations of momentum, mass, and energy conservations as well as turbulence kinetic energy equation sequentially alongside. In order
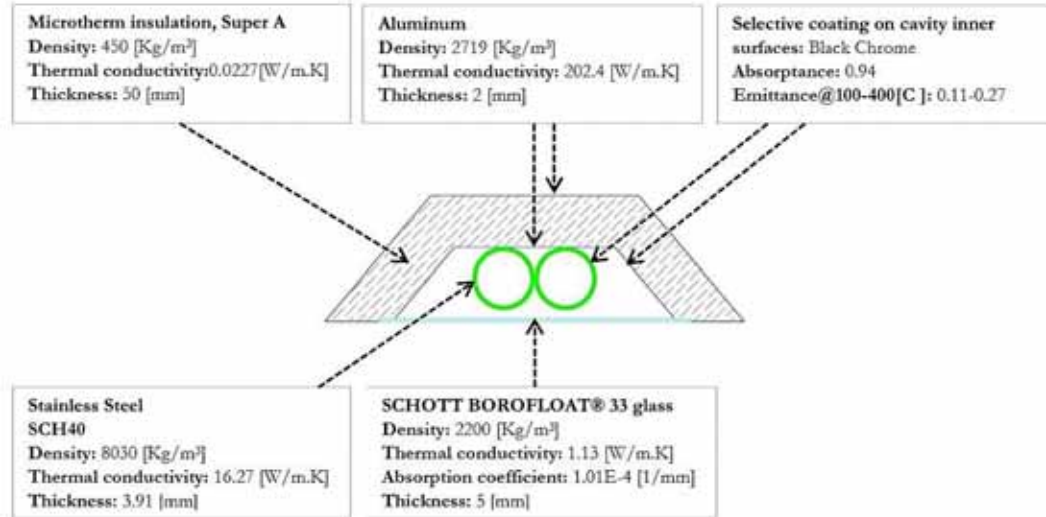

to study the natural convection inside the cavity, the gravitational acceleration should be included in the calculations. The viscous model is RNG k-ε, and the radiation model is the DO model, which works across the full range of optical thickness but with a higher demand on the computational resources (Fluent, 2011).

Fig.7: Material properties

Boundary conditions: In all CFD cases, the wind is blowing at a constant speed of 5 m/s – design criterion to study stratification when the heat loss rate is relatively high– from left to right normal to longitudinal axis of the receiver. The cavity inner gas content and pressure are patched differently in ANSYS Fluent in order to perform the parametric studies over these parameters. Each tube is virtually divided into two parts: upper half and bottom half. To study the stagnation temperature, the heat flux obtained from the optical analysis is introduced only at the bottom half of the tubes whereas to determine the heat loss rate, the absorber temperature is assumed to be uniform. The highest attainable stagnation temperature is considered for an altitude angle of 90° and air is treated as an ideal gas in the CFD model.

4.2 CFD Results

Velocity contours visualization: As Fig.8 illustrates, the mesh size is appropriate to detect the boundary layer and separation at the upper and lower edges of the trapezoid. Moreover, no uniform natural convection is observable and spots with relative higher velocities are merely seen locally in a small region between the
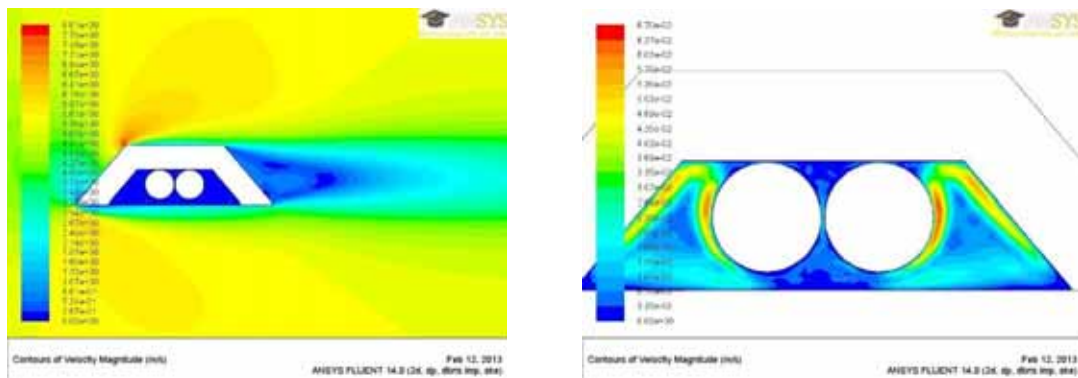
sides of the trapezoid and the absorber tubes.

Fig.8: Contours of velocity magnitude around (left) and inside (right) of the cavity filled with atmospheric air, 90° altitude angle

Temperature contours visualization: Contours of static temperature and radiation temperature are illustrated in Fig.9 when the absorber is at the design temperature equal to 212 °C. According to the results, the insulation thickness (50 mm) is adequate to provide a proper thermal resistance between the inner and outer surfaces of the cavity. Furthermore, the stratification condition is recognizable inside the cavity at the atmospheric pressure from the highest temperature in the spots adjacent to the absorber tubes to the lowest one in the regions close to the glass at the bottom. The results are in agreement with the results of velocity contours (Fig.8) presented before that shows almost still air with local velocity gradients in few spots. The stratification condition ensures natural convection alleviation inside the cavity. Besides, the temperature variation on the inner and outer surfaces of the glazing, illustrated in Fig 10, confirms the sufficient gap (8 mm) between the glass and hot surfaces of the absorber to protect the glazing from high temperatures.
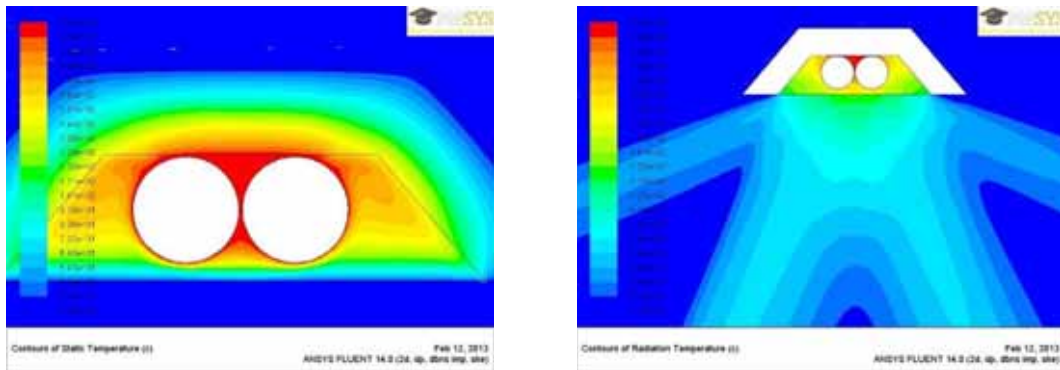

Fig.9: Contours of static temperature (left) and radiative temperature (right) for the cavity filled with atmospheric air, 90°
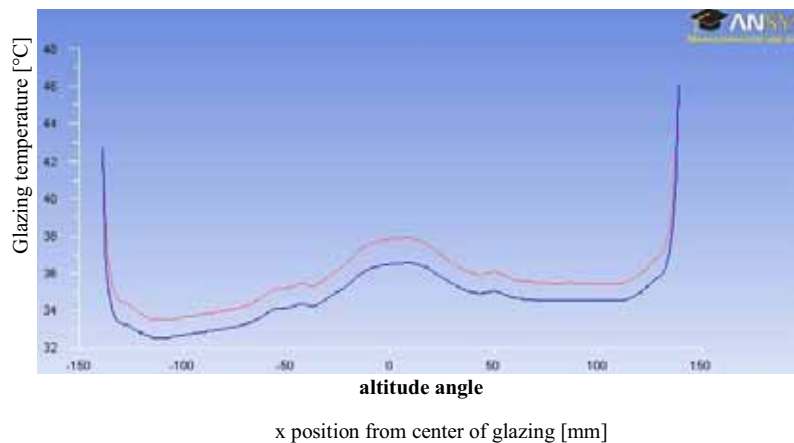

x position from center of glazing [mm]
Fig.10: Static temperature distribution on inner and outer surfaces of the glazing, T$_{absorber}$=212 °C

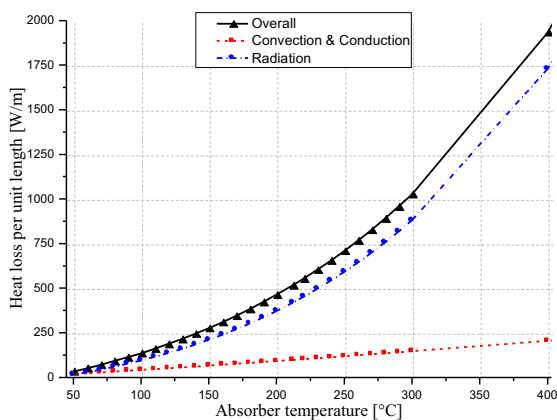**Fig.11: Heat loss rate vs. absorber temperature**

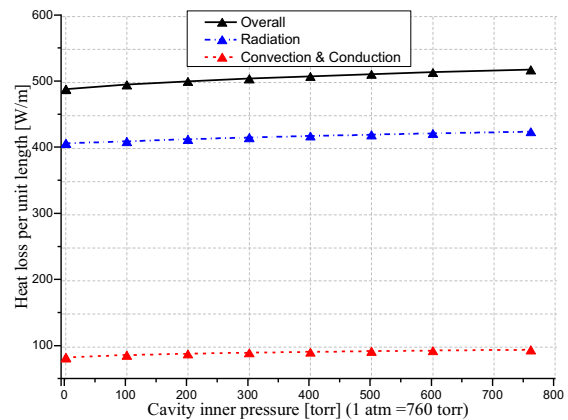**Fig.12: Heat loss rate vs. pressure, T$_{absorber}$=212 °C**

Heat loss rate vs. absorber temperature: The heat loss per unit length of the receiver is studied for the atmospheric cavity charged with air when the absorber temperature varies within the range 50 to 400 °C. Using an efficient insulation material gives rise to a comparatively small participation of the mixed

conduction-convection losses over a wide range of absorber temperatures; consequently as Fig.11 offers, the overall trend of heat loss is mainly imposed by the radiation loss.

Heat loss rate vs. inner pressure: The sensitivity analysis is performed over inner pressure of the cavity when the absorber temperature is fixed at 212 °C. Considering the results in Fig.12 highlights that only 6% reduction is achieved over a wide range of inner air pressure from 0.01 to 760 torr (1 atm = 760 torr). This finding is also consistent with the observed stratified condition at the atmospheric pressure. Moreover, reducing the inner pressure is expected to have a large impact on diminishing natural convection inside the cavity that is already sufficiently achieved even at the atmospheric pressure. Thus, there is no need to use durable airtight materials that are indispensable to maintain semi-vacuum inner pressure.

Heat loss rate vs. absorber temperature in the cavity filled with atmospheric inert gas: Fig.13 compares the heat loss rate of air with some inert gases namely argon and nitrogen within the temperature range from 100 to 300 °C. Comparing the results in Tab.4 shows a slight decrease of 6% in the overall heat loss rate for argon than of air, which can be explained by lower conductivity of argon under stratification together with lower local velocities in the cavity. As discussed earlier, the radiation still remains the dominant heat loss mechanism with minor changes in all cases.

Tab.4: Comparison of heat loss rate for air, argon, and nitrogen, $T_{absorber}$=212 °C

Cavity Gas Content	Glass Temp. [°C]		Velocity [cm/s]		Total heat loss rate [W/m]	Radiative heat loss rate [W/m]	Radiation portion [%]
	Max.	Min.	Max.	Min.			
Air	43.76	33.50	0.62	2.17E-03	516.2	418.6	81.1
Argon	40.98	29.85	0.56	3.02E-03	486.4	400.2	82.3
Nitrogen	43.32	29.91	0.13	6.34E-04	489.2	400.5	81.9

Stagnation temperature: The results for absorber and glazing temperatures at stagnation are shown in Fig.14 for the altitude angle 90°, where the inner pressure varies from 0.01 to 760 torr. A minor temperature drop is detected from 810 °C at the atmospheric pressure to 804 °C at the lowest studied pressure. It is concluded that the stagnation temperature dependency on inner pressure is not significant. This can be explained by the dominant effect of the radiation loss in the current model, which is almost independent from
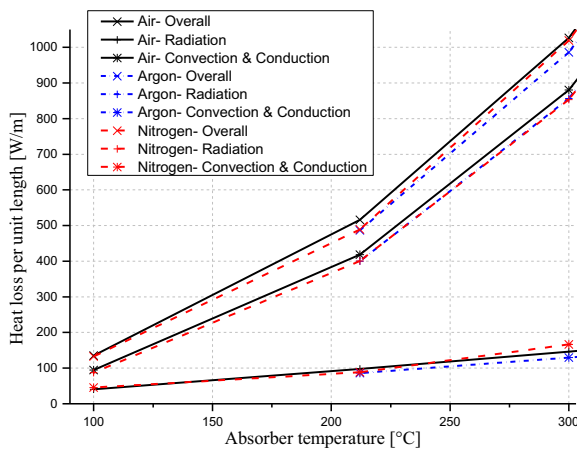
the inner pressure.

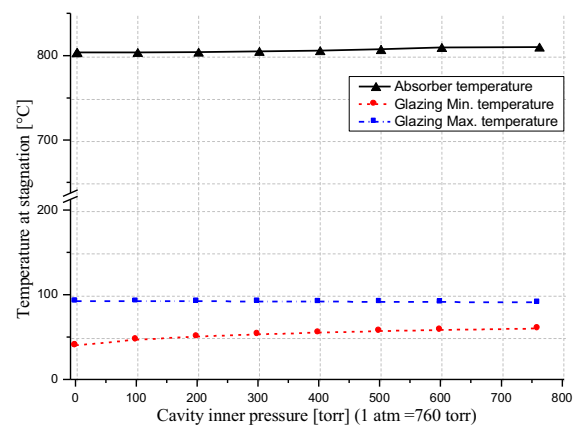**Fig.13: Heat loss rate vs. absorber temperature**   **Fig.14: Stagnation temperature vs. cavity inner pressure**

4.3 Non-Glazed and Increased-Depth Configurations

Two more cases: Non-glazed and Increased-depth, are modeled to ascertain and compare the strength of the main contributing factors on overall heat loss, namely forced convection and radiation. The geometry in the Non-glazed case is exactly similar to the original design (Fig.3) but without the underneath glazing. In the next case, the depth of the cavity is increased by extending the trapezoidal sides so that the incident radiation on the first row of mirrors is not blocked by the extended sides. The additional parts are shown in red in Fig.15. Here, the aim is to hinder the wind stream around the absorber and, hence, an improvement in diminishing the convective heat loss compared to non-glazed case is expected at a lower cost.

4.4 Comparison:

Conductive and convective heat loss rate: The results are illustrated in Fig.16, the first studied case gives significantly lower heat loss with slight growth over a wide range of temperature proving the effectiveness of using the glazing and insulation in suppressing convection and conduction losses. Furthermore, an improvement is also apparent in the Increased-depth case compared to the Non-glazed one due to lower air velocities around the absorber.

Radiative heat loss rate: As Fig.17 illustrates, the radiation losses in the two first cases are comparable as the geometry and consequently the shape factor is nearly the same due to the fact that the glass is optically transparent with small absorption / reflection coefficients. However, the third case with an increased depth has lower radiation heat loss as the extended surfaces hinder the radiation to the surrounding, albeit the difference becomes negligible at low operating temperatures.

Overall heat loss rate: The results for overall heat loss rate have been compared in Fig.18 which present
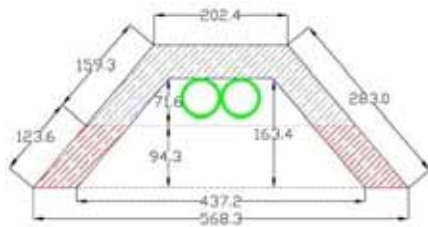

dominantly lower values for the glazed case as predicted.

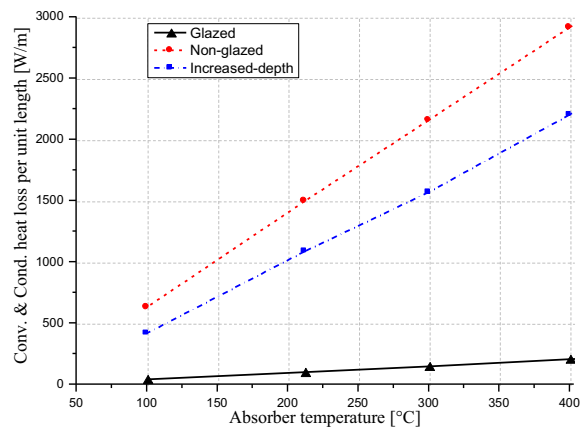**Fig. 15: Increased-depth case configuration (unit: mm)**   **Fig.16: Conductive / convective loss vs. absorber temperature**

Fig.17: Radiative heat loss rate vs. absorber temperature   **Fig.18: Overall heat loss rate vs. absorber temperature**

5.   Conclusion

According to the results, an eight millimeter gap between the absorber and underneath glazing is adequate to protect it from the high temperature of the absorber (450°C and above) that might be reached at low flow rates prior to complete stagnation. Moreover, the insulation thickness is sufficient to create proper thermal resistance at the maximum operating temperature (212 °C). Studying the velocity contour in conjunction with the non-radiative heat dissipation behavior within the studied inner pressure range (0.01 to 760 torr) proves that a well-stablished stratification is achievable even in the atmospheric air-filled cavity. This being due to the fact that the absorber tubes act as a hindrance against natural convection so long as their cross sectional area is large compared to the inner gross area of the cavity. As a result of diminishing the
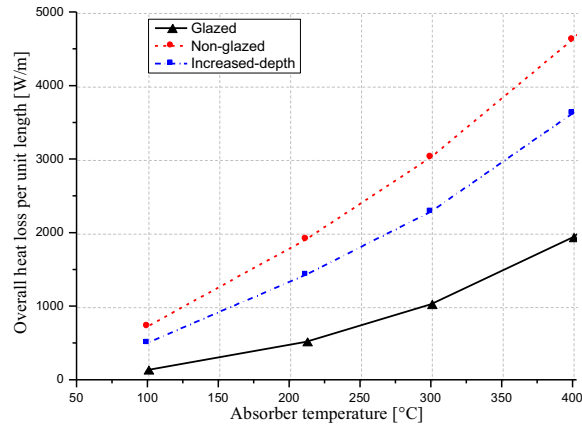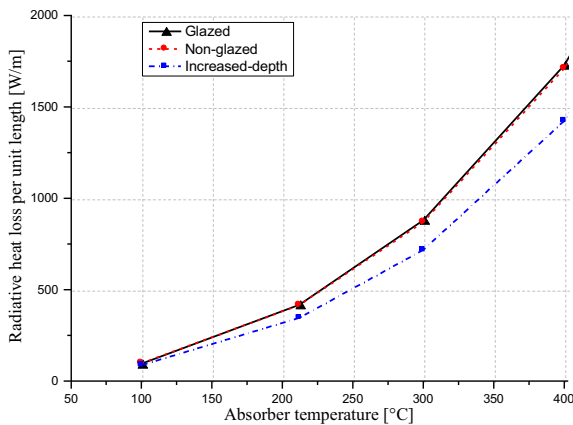
conduction and convection losses in the model, the secondary radiation loss part (long wavelengths) from the inner parts of the cavity becomes dominant by allocating 82% of the overall heat loss. This study highlights the importance of reducing the long-wave radiative loss from the receiver to the surrounding to achieve high performance. The influence of the radiative part becomes dominant when the conductive and convective losses are efficiently suppressed in a well-insulated receiver with a proper inner stratification state. The solution might lie in using more efficient selective coating materials, with higher absorption and lower emissivity factors, along with employing advanced transparent coating materials on the glazing to reflect back the long wavelengths to the cavity. However, further study is needed to assess the efficacy of each method depending upon the properties of the materials used.

6. References

Callister, Jr, W. D. & Rethwisch, D. G., 2010. Materials Science and Engineering, An Introduction. 8th ed. s.l.:John Wiley & Sons, Inc.

Duffie, J. & Beckman, W., 1991. Solar engineering of thermal processes. Second ed. New York: John Wiley & Sons, INC.

Fluent, 2011. Ansys Fluent User's Guide. Canonsburg(Pennsylvania): Ansys,Inc.

Forristall, R., 2003. Heat Transfer Analysis and Modeling of a Parabolic Trough Solar Receiver Implemented in Engineering Equation Solver, Colorado: NREL(National Renewable Energy Laboratory).

Lambda, R. C., 2012. TracePro User Manual. s.l.:Lambda Research Corporation.

Microtherm®, 2011. Insulation solutions for Concentrated Solar Power. [Online]
Available at: http://www.microthermgroup.com

Schott, 2012. SCHOTT Technical Glass Solutions GmbH, Jena: Schott Solar.

Shin Yee, W., 2006. CFD Modelling of a Continuous Baking Oven and Its Integration with Controller Design, s.l.: National University of Singapore, Department of Chemistry.

Weiss, W. & Rommel, M., 2008. Process Heat Collectors-State of the Art within Task33/IV-IEA SHC-Task 33 and SolarPACES-Task IV, Austria: AEE INTEC.